Computer Networks 83 (2015) 45–58

Contents lists available at ScienceDirect

Computer Networks

journal homepage: www.elsevier.com/locate/comnet

Measurement-based coverage function for green femtocell networks

Anna Dudnikova *, Daniela Panno, Antonio Mastrosimone

Department of Electrical, Electronics and Computer Engineering, University of Catania, Catania, Italy

ARTICLE INFO

Article history:
Received 5 August 2014
Received in revised form 20 January 2015
Accepted 26 February 2015
Available online 6 March 2015

Keywords:
LTE femtocell
Dynamic adaption
Self-optimization
Energy efficiency
Power management
Offloading

ABSTRACT

In this paper, we propose a self-optimized coverage function for LTE femtocells embedded in a macrocell area. Each Femto Base Station (FBS) adapts its pilot power, and thus the coverage, to the on-site traffic demand. Under low traffic conditions the FBSs, whose presence is not essential for the proper operation of the network, reside in a low power Listen Mode. In this way a relevant energy saving on entire femtocell network can be achieved. In a high-load scenario, FBSs dynamically create high capacity zones under interference constraints. This permits to improve system capacity and offload more traffic from the nearby macrocell and, in the same time, to minimize co-channel interference in the femtocell tier.

1. Introduction and related works

Femtocell concept has found a place in the architecture of LTE networks as a cost-effective solution designed to improve both the coverage and the user throughput indoors (where mobile users spend most of time), as well as the overall system capacity by offloading data traffic from macrocells. Femtocells were originally conceived to be installed by terminal consumers without network preplanning in private households. At present time, it is increasing the adoption of femtocells from the enterprise segment, which is a key focus for a growing number of operators.

According to the researches of "Informa Telecoms & Media", the 9.6 million femtocells in operation today make up 56% of all base stations (BSs) globally and they will continue to outnumber all other types of cells with an expected 86% of the total BS market in 2016 [1]. Due to the massive deployment of these additional BSs the wireless network energy consumption might be significantly increased. This problem becomes especially acute in public areas (e.g. airports, shopping malls, etc.) characterized by a large number of mobile users, which require high data rates. In these environments, the capacity of a macrocell is not enough and a very high femtocell density is expected. Let's also note that the user number is highly variable. For this reason the use of the static pilot power configuration, in which FBSs are required to transmit pilot signals continuously and to do the related processing even when they are not serving any users, would lead to considerable energy waste for entire femtocell network under low traffic load conditions. Therefore, energy saving techniques need to be exploited by designing efficient mechanisms to enable sleep modes in FBSs.

Another significant issue arises from the fact that femtocells are typically configured to use the same licensed frequency band as macrocells with which they coexist. This is spectrally efficient, but can cause interference issues that become more challenging in dense FBS

* Corresponding author.
E-mail addresses: anna.dudnikova@dieei.unict.it (A. Dudnikova), daniela.panno@dieei.unict.it (D. Panno), antonio.mastrosimone@dieei.unict.it (A. Mastrosimone).

http://dx.doi.org/10.1016/j.comnet.2015.02.025
1389-1286/

deployments (e.g. in enterprise environments), where femtocells are very likely to be overlapped. The increased level of interference leads to a significant performance degradation of the overall femtocell network.

For the success of dense femtocell networks, both the issues of energy efficiency and intercell interference mitigation should be addressed together optimizing the potential conflicts while, at the same time, trying to minimize the intervention of network operator/user.

Many works in the literature (e.g. [2–6]) have dealt with the above issues separately, neglecting the impact of their simultaneous optimization. In [2–4] only the energy saving issue is addressed, while the interference between adjacent femtocells is not taken into account. These works assume a constant femtocell radius in the downlink irrespective of surrounding radio frequency (RF) environment and femtocell deployment topology, and they propose to switch off unnecessary hardware components of FBSs when not involved in an active call. In [5,6] adaptive coverage control schemes are presented, but the energy saving issue is not addressed.

Other works have proposed solutions aiming at optimizing the two objectives simultaneously. In [7], the scheme includes UE-controlled sleep mode for FBSs in order to reduce power consumption. The FBS that receives the strongest wake-up signal, broadcasted by UEs, is chosen by Femtocell Management Unit to be waken-up. Then each active FBS adapts its transmission power as a function of UEs positions. In [8] FBSs use user activity detection in order to save energy. Active FBSs adjust their pilot power levels in order to minimize co-tier interference following commands of a Femtocell Interference Unit. Both these proposals operates in a centralized fashion which envisages a local femtocell management unit. So, they exploit the advantage of the centralized knowledge of the overall state of the network to implement the optimization strategy. However this results in an increased complexity of the system, mainly due to the need of a central controller and to the information exchange between femtocells and the controller itself, which may cause signaling overhead. Moreover, centralized implementations typically suffer of low scalability and robustness, thus making them not attractive for practical use in expected large-scale femtocell deployment.

In this paper we deal with these problems by proposing a distributed self-configuration approach. It aims at addressing both energy consumption reduction and femto–femto interference issues without requiring a leader or a central control unit, neither information exchange between the base stations of the network. In the proposed algorithm (an improved version of the one presented in [9,10]) we make use of radio measurements integrating in each FBS automatic and autonomous procedures of configuration and optimization of coverage according to the detected on-site user activity. The adaptive nature of the coverage algorithm allows to increase the capacity and the Energy Efficiency (EE) of the overall network. The simulation results show the flexibility, the scalability, the robustness and the stability of our method. Furthermore, we make use of a component-based model to quantify the energy saving achieved by our algorithm taking into account a typical diurnal traffic pattern in a public area.

The paper is organized as follows: in Section 2, the network model and the problem formulation are defined; in Section 3 the detailed description of the proposed power control algorithm is given; in Section 4 the performance of our algorithm is evaluated by MATLAB simulations. Concluding remarks are given in Section 5 and are followed by the Appendix which is dedicated to the decision-making parameters for our algorithm.

2. Network model and problem formulation

In the following a two-tier heterogeneous network comprising a single macrocell embedded with a set of FBSs is considered (Fig. 1). Both FBSs and the Macro Base Station (MBS) are assumed to operate using the same OFDMA technology and to use the same licensed frequency band. We assume that the MBS ensures complete coverage, as this is the case in dense public areas where femtocells are likely to be deployed as hotspots of large capacity for the purpose of increasing the throughput and offloading traffic from macrocells. Femtocells are deployed without cell pre-planning and all BSs are equipped with omni-directional antennas. For convenient analysis, some assumptions are made and are listed below.

Assumption 1. There is no intra-cell interference in the downlink.
Assumption 2. For FBSs the open access mode is adopted, i.e. FBSs behave as regular BSs and are accessible by any UE. This access mode is considered to be used widely for enterprise deployments, in shopping malls, cafes and other public areas [11,12].
Assumption 3. Each UE can be served by at most one BS. Cell selection is based on a maximum downlink received power of pilot signal.
Assumption 4. FBSs operate in two modes: Listen Mode and Active Mode [4].

Based on "Assumptions 2 and 3", the macro–femto interference is less acute than femto–femto interference. In fact in this scenario UEs which are causing or suffering from interference can be handed over freely between the macro and femtocells [13]. Furthermore, specific macro–femto interference mitigation approaches (e.g. [14–17]) can be additionally applied without deteriorating the performance of our power control scheme. For this reason we focus only on the problem of interference in the femtocell tier.

In regard to the femto–femto interference avoidance schemes, there are two different approaches: those that use intelligent allocation of spectral resources (Physical Resource Blocks (PRBs) in the LTE specifications) [18–20] and those that apply the femtocell pilot power calibration to minimize femtocell overlapping [21,22]. We follow the second approach, therefore we do not take into account the allocation of PRBs to single active UEs' connections. However, the strategies of intelligent resource allocation can be used together with our pilot power control so as to improve the quality of both. In this paper we propose an algorithm that performs a self-optimization coverage

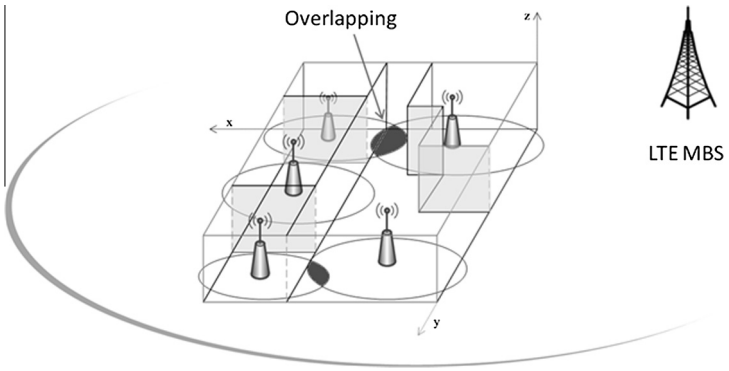

Fig. 1. Scenario: dense femtocell deployment.

function that continuously adapts the pilot power and thus the coverage of femtocells in order to fulfill the following objectives:

(1) Improve EE of the femtocell network in a low load scenario.
(2) Improve the overall system capacity in high load conditions and offload more traffic from the outdoor macrocell by maximizing the femtocell coverage.
(3) Reduce co-channel interference between adjacent femtocells by minimizing the coverage overlaps with the view of providing a minimum level of Quality of Service (QoS) to all femtocell users.
(4) Provide a robust, flexible, scalable and stable control scheme suitable for a large-scale femtocell deployment.

To accomplish the fourth objective, we have chosen a self-organizing measurement-based control scheme without any signaling exchange between BSs. Thanks to this last feature, the delay introduced by Internet as backhaul for the FBS has no effect on the operation of our control scheme.

The stability of our algorithm was obtained considering that the femtocell size does not have significant impact on the energy consumption of the FBS [23]. So, once an active FBS has adapted its configuration to the current traffic demand, it switches to Stabilization State rather than continuously adapt its pilot power as a function of users' positions (that may result in an increased number of computational processes and handovers).

3. Pilot power control algorithm

In this section we present the description of the algorithm in regard to a single FBS_k. Fig. 2 illustrates the FBS's State Diagram and synthesizes the whole proposed power control mechanism.

Femtocells can reside in two principal operation modes: Listen Mode and Active Mode. The FBS that resides in Listen Mode disable its pilot power and associated processing, thus it achieves a significant energy saving. In Active Mode the FBS dynamically calibrates its pilot power

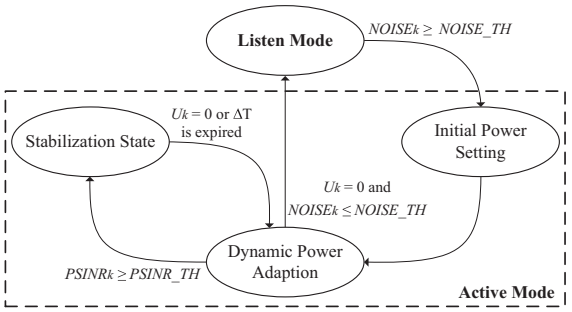

Fig. 2. State diagram in regard to a single FBS_k.

(and thus the coverage) as a function of local traffic demand by carrying out a two step procedure that includes Initial Power Setting and Dynamic Power Adaption. As soon as an optimal configuration is achieved, the FBS passes to Stabilization State with constant setting of the pilot power.

Operation of the proposed algorithm is based on estimation of two decision-making parameters by FBS_k:

(1) the noise level on the uplink frequency band ($NOISE\_UL_k$) measured by the FBS_k for detecting the presence of any active user;
(2) the ratio between pilot signal and interfering pilot signals plus noise for detecting harmful interference ($PSINR_k$, Pilot Signal to Interference plus Noise Ratio) and minimizing the cell overlap.

The detailed description of the decision-making parameters is given in Appendix. By comparison of these estimated values with the corresponding thresholds (*NOISE_TH* and *PSINR_TH* respectively) each FBS makes a decision on its pilot power calibration. Below we provide the detailed description of the algorithm.

3.1. Listen mode

In the initial state, when the local traffic demand is low or absent, the FBS without any active call resides in a low

power Listen Mode. Femtocell activity is controlled by a low-power sniffer integrated in the FBS, that continuously performs measurements of $NOISE\_UL_k$. When a UE, located inside the sensing range of the sniffer, connects to the MBS, the sniffer detects a rise of the received noise power and the presence of active user can be detected. To avoid an unreasonable activation of idle femtocells we have introduced a threshold value of noise level ($NOISE\_TH$), which allows to control the sensitivity of FBSs.

3.2. Initial power setting

When the sniffer detects an adequate rise in the received noise power on the uplink frequency band, that is $NOISE\_UL_k > NOISE\_TH$, the FBS_k switches on its pilot transmission and the associated processing, providing cell coverage with initial radius R_{ini}. For this purpose, the FBS sets the initial transmit power to such a value that a user located at the edge of the femtocell with radius R_{ini} receives, on average, the same power from the FBS and from nearby MBS. Therefore, the initial femtocell pilot power, subject to the maximum limit power of the FBS $P_{f,max}$, can be calculated in dBm as in [24]

$$P_{k,ini} = min(P_{r,k}^{MBS} + PL(R_{ini}), P_{f,max}), \quad (1)$$

where $P_{r,k}^{MBS}$ is the pilot power of MBS received by FBS_k; $PL(R_{ini})$ is the estimated path loss from the femtocell to a UE at the target radius R_{ini}.

The received power $P_{r,k}^{MBS}$ is not estimated using a path-loss model, but it is measured using the built in measurement capability of the FBS. This approach has the advantage that no information on the macrocell network is required.

Then, active UEs located within the coverage of FBS_k can detect the presence of two BSs, macro and femto, and can make a handover based on "Assumption 3". Users offloaded to the femtocell have larger peak throughputs as they are close to their serving BS. In addition, those UEs who are still connected to the MBS enjoy more resources as they are shared now with a fewer number of macrocell users.

3.3. Dynamic power adaption

The Initial Power Setting procedure described above, which provides the initial cell coverage of the FBS, is optimized by Dynamic Power Adaption scheme. Iteratively, FBS_k estimates the decision-making parameters ($NOISE\_UL_k, PSINR_k$), compares them with corresponding thresholds and calibrates its pilot power accordingly until finding an optimal power configuration which accomplishes the objectives 2 and 3 of Section 2. The coverage optimization process is summarized in Table 1. Below we list all the considered cases and provide some explanatory notes.

(1) ***There are active UEs linked to the FBS_k, i.e.*** $U_k \neq 0$
(1.a) $NOISE\_UL_k \geqslant NOISE\_TH$ & $PSINR_k \geqslant PSINR\_TH$
If both decision-making parameters exceed corresponding thresholds, it means that there are other active UEs connected to the MBS in the sensing range of the sniffer and in the same time the minimum QoS requirement of each own active UE is ensured. In this case FBS_k has to increase its cell radius, $R_k(i-1)$, of ΔR^+ aiming to provide the coverage to more UEs. Accordingly, FBS_k adapts its pilot power as follows

$$P_k(i) = min(P_{r,k}^{MBS} + PL(R_k(i)), P_{f,max}), \quad (2)$$

where i is the iteration number.
Then the active UEs, that detect pilot transmission of more BSs, can make a handover based on "Assumption 3".
In the next iteration the FBS will update the decision-making parameters and will verify the fulfillment of one of the conditions (1.a, 1.b, 1.c, 2.a, 2.b).
(1.b) $PSINR_k \leqslant PSINR\_TH$
A $PSINR_k$ value below its acceptable level means that the minimum QoS requirement is not satisfied for at least one currently connected user. This user is likely to be located in the overlap area between adjacent femtocells. So FBS_k decreases its cell radius of ΔR^- by setting its pilot power in the following way:

$$P_k(i) = max(P_{r,k}^{MBS} + PL(R_k(i)), P_{f,min}), \quad (3)$$

where $P_{f,min}$ is a minimum transmit power of the FBS.

Table 1
Dynamic power adaption.

Definition: U_k is a number of active users linked to the FBS_k
Initialize: $Stabilization\ State \leftarrow FALSE$

```
while Stabilization State ← FALSE do
    Update NOISE_UL_k and U_k;
    if U_k ⩾ 1 then
        Update PSINR_k ;
1.a     if NOISE_UL_k ⩾ NOISE_TH & PSINR_k ⩾ PSINR_TH
        then
            Increase pilot power:
            R_k ← R_k + ΔR^+ ⇒ P_k ← min(P_{r,k}^{MBS} + PL(R_k), P_{f,max});
        end
1.b     if PSINR_k < PSINR_TH then
            while PSINR_k ⩽ PSINR_TH do
                Decrease pilot power:
                R_k ← R_k − ΔR^− ⇒ P_k ← max(P_{r,k}^{MBS} + PL(R_k), P_{f,min});
                Update PSINR_k;
            end
            No power modification: R_k ← R_k ⇒ P_k ← P_k;
            Stabilization State ← TRUE;
        end
1.c     if NOISE_UL_k < NOISE_TH & PSINR_k ⩾ PSINR_TH
        then
            No pilot power modification: R_k ← R_k ⇒ P_k ← P_k;
            Stabilization State ← TRUE;
        end
    else
2.a     if NOISE_UL_k ⩾ NOISE_TH then
            if P_k < P_{f,max} then
                Increase pilot power:
                R_k ← R_k + ΔR^+ ⇒ P_k ← min(P_{r,k}^{MBS} + PL(R_k), P_{f,max});
            else
                Turn off pilot transmission: R_k ← 0 ⇒ P_k ← 0;
                Return to Listen Mode processing, break;
            end
        else
2.b         Turn off pilot transmission: R_k ← 0 ⇒ P_k ← 0;
            Return to Listen Mode processing, break;
        end
    end
end
```

As a result of coverage reduction, those users who were suffering from the interference appear to be out of coverage of FBS_k and they establish a new connection based on "Assumption 3".

In the next iteration the FBS updates $PSINR_k$ value and verifies the fulfillment only of condition (1.b). So FBS_k continually decreases its pilot power until $PSINR_k \geqslant PSINR\_TH$ (irrespectively to $NOISE\_UL_k$ value), then switches to Stabilization State. This decision allows to eliminate continuous coverage fluctuations in order to avoid an excessive number of handover events.

(1.c) $NOISE\_UL_k < NOISE\_TH$ & $PSINR_k \geqslant PSINR\_TH$

FBS has achieved an optimal coverage and it switches to Stabilization State.

(2) ***No active UE linked to the FBS$_k$, i.e.*** $U_k = 0$

If there are not currently connected active UEs, FBS_k adapts its coverage according only to $NOISE\_UL_k$ value.

(2.a) $NOISE\_UL_k \geqslant NOISE\_TH$

It means that there are active macro UEs located in the sensing range of the sniffer.

If $P_k \leqslant P_{f,max}$, the FBS increases its pilot power according to (12). Due to the coverage extension some active macrocell users can handover into the femtocell based on "Assumption 3". In the next iteration the FBS updates the decision-making parameters and verifies the fulfillment of one of the conditions (1.a, 1.b, 1.c, 2.a, 2.b), adapting its pilot power setting accordingly.

If FBS_k has achieved the maximum value of its pilot power ($P_k = P_{f,max}$), while macro UEs remain unattainable ($U_k = 0$), FBS_k turns off its pilot power and associated processing and rests in Listen Mode for ΔT time interval. So, FBS_k will reside in an energy saving state, rather than being active measuring a high $NOISE\_UL_k$ level due to transmissions of unattainable UEs.

(2.b) $NOISE\_UL_k < NOISE\_TH$

The FBS turns off its pilot transmission and associated signaling and returns to the Listen Mode processing.

3.4. Stabilization state

The FBS achieves Stabilization State when its pilot power (and thus the coverage) is optimized based on the on-site traffic demand and in the same time an acceptable SINR level is guaranteed to each of its currently connected user. From Stabilization State, FBS_k switches to Dynamic Power Adaption procedure in order to detect changes of the local radio environment and, if required, updates its pilot power setting. The transition to Dynamic Power Adaption is carried out: periodically with time intervals ΔT if there are active UEs currently connected to FBS_k or immediately when no UE is connected to FBS_k, i.e. $U_k = 0$ is verified.

4. Performance evaluation

In this section we verify the performance of the proposed scheme by simulations in MATLAB.

4.1. Simulation assumptions and performance metrics

In the simulations the system parameters were set as shown in Table 2. More specifically, some assumptions and simplifications were made: all UEs have "Power class 3" ($P_{max} = 23$ dBm), defined by the standard; all FBSs have the same maximum transmission power $P_{f,max}$; P_0 and α values are equal for all FBSs; UEs belong to two different traffic classes: Low-Rate users and High-Rate users with different number of allocated Physical Resource Blocks (PRBs).

As regards the traffic load, in our simulations we consider N_u active UEs (50% are Low-Rate users and 50% are High-Rate users) uniformly distributed, or, alternatively, concentrated in the macrocell area.

Furthermore, we have defined the following metrics.

(1) Overlapping factor of femtocells (Θ).

$$\Theta = \frac{\sum_{i=1}^{N}\sum_{j=i+1}^{N}\Theta_{i,j}}{\sum_{i=1}^{N}A_i - \sum_{i=1}^{N}\sum_{j=i+1}^{N}\Theta_{i,j}}, \tag{4}$$

where N is the total number of FBSs; A_i is the area covered by femtocell i; $\Theta_{i,j}$ is the overlap area between femtocell i and femtocell j.

(2) Percentage of users present in the macrocell area served by all FBSs (Φ).

$$\Phi = \frac{\sum_{i=1}^{N}U_i}{N_u} \cdot 100, \tag{5}$$

where U_i is a number of users served by FBS_i; N_u is a total number of active users present in the macrocell area.

In the following for assessing the performance of our coverage function we compare it to the static pre-planned configurations, where the pilot power of each FBS is fixed and is ideally set to provide the maximum coverage with minimal femto–femto interference by excluding overlap between adjacent femtocells.

Table 2
System parameters.

Parameter	Symbol	Value
Initial femtocell radius	R_{ini}	7 m
Maximum transmit power of FBS	$P_{f,max}$	23 dBm
Minimal transmit power of FBS	$P_{f,min}$	−40 dBm
Transmit power of MBS	P_t^{MBS}	43 dBm
PRBs assigned to a High-Rate user	M_u	3
PRBs assigned to a Low-Rate user	M_u	1
Maximum transmit power of UEs	P_{max}	23 dBm
Path loss compensation factor	α	1
Power to be contained in one PRB	P_0	−106 dBm
Path loss at 1 m	A_S	37 dBm
Path loss exponent	n	3
Thermal noise power	N_0	−96.8 dBm
Wall penetration loss	L_w	12 dB
Number of FBSs	N	5
Range modification step	ΔR^+	2 m
	ΔR^-	1 m

4.2. Determination of thresholds

The proposed algorithm requires to set thresholds' values: *PSINR_TH* and *NOISE_TH*. With regard to the first parameter, in Appendix B we show that the estimated *PSINR* value is the worst SINR which an active femto user could suffer. LTE specifications [25] indicate SINR = −4 dB as the minimum requirement to guarantee an acceptable QoS. As our coverage control ensures in each femtocell that no UE's *PSINR* falls below its threshold level, we have chosen to set *PSINR_TH* equal to −4 dB for providing a minimum acceptable QoS to all femto users.

With this value of *PSINR_TH* we have carried out a series of simulations in order to determine an optimal *NOISE_TH* level. The scenario that we have used represents an enterprise environment with 5 FBS localized so as to cover most part of an area (60×40 m^2). We also assume that this area is covered by a MBS located at a distance of about 300 m.

Figs. 3 and 4 show diagrams of Θ and Φ, respectively, for *NOISE_TH* varying from −60 to −50 dBm. The results are averaged over 50 independent simulation runs. For the static configuration $\Theta = 0$ for different traffic load scenarios, this is because the pilot power of each FBS is constant and it is configured to avoid overlap areas between adjacent femtocells. The value of Φ, instead, is maintained around 73%. So, even such "ideal" configuration cannot guarantee the coverage to all active UEs present in the considered macrocell area. By comparative analysis of the simulation results (see Figs. 3 and 4), it can be estimated that a good trade-off between Θ and Φ is achieved with *NOISE_TH* set to −53 dBm. In fact, this threshold value provides $\Theta \leqslant 5\%$ and Φ is about 80% in a high load scenario.

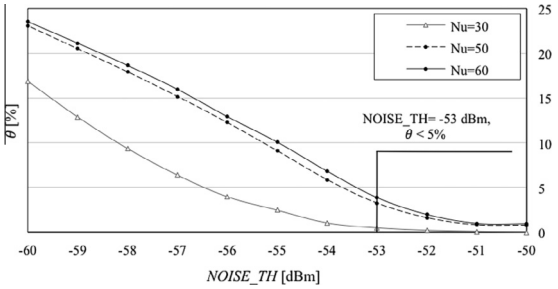

Fig. 3. Overlapping factor of femtocells (Θ) vs. *NOISE_TH*.

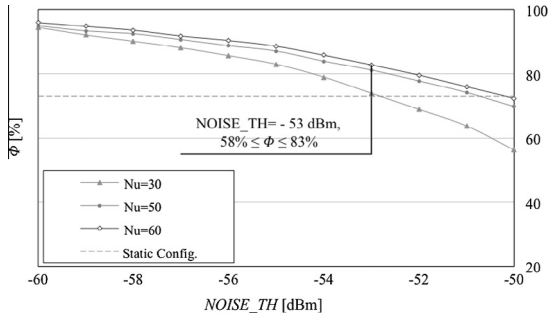

Fig. 4. Percentage of users served by FBSs (Φ) vs. *NOISE_TH*.

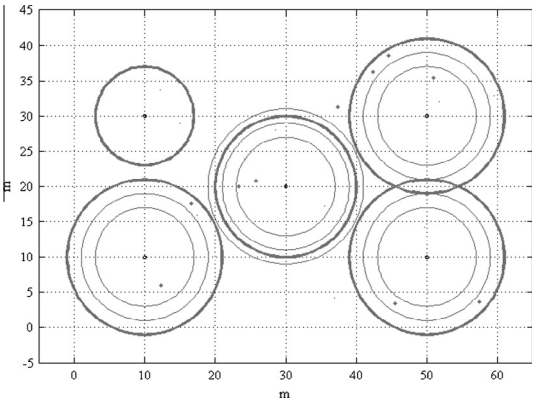

Fig. 5. Example of the operation of the proposed algorithm.

Finally, the thresholds are set to: *PSINR_TH* = −4 dB; *NOISE_TH* = −53 dBm. With this values of thresholds in Fig. 5 is shown an example of the operation of our algorithm: each FBS dynamically adapts its pilot power (fine line) according to the traffic demand until Stabilization State (bold line). Here and in all following simulation results the users present in the macrocell area are indicated by dots.

4.3. Evaluation of scalability and robustness

To evaluate the scalability and robustness of our proposal, we have carried out a series of simulations varying the network topology:

Topology 1. 5 FBS localized so as to cover most part of an area (60×40 m^2);
Topology 2. 3 FBS localized so as to cover most part of an area (60×40 m^2);
Topology 3. 20 FBS randomly distributed in an area (100×100 m^2).

For all topologies, the MBS is assumed to be located at the distance of about 300 meters.

In Figs. 6 and 7 are shown Φ and Θ for each topology at various UE's densities per unit area (ρ = activeusers/m^2). When the system is in low traffic conditions ($\rho \leqslant 0.01$), our algorithm provides lower Φ values compared to the static configuration, as in this case our power control scheme places some FBSs in Listen Mode (for instance, three FBSs reside in Listen Mode in Fig. 8), thus allowing to achieve a relevant energy saving on entire femtocell network. However, in this scenario the MBS can alone handle the traffic while offering to users satisfactory throughput. When the traffic load increases ($\rho > 0.01$) the proposed algorithm, thanks to its adaptive nature, allows to obtain higher Φ values compared to the static configuration (see Fig. 6), while maintaining an acceptable level of Θ (see Fig. 7). More precisely, in Fig. 9 is shown an example of how the algorithm is able to provide the coverage to those users (indicated by triangles) who could not be covered by the static configuration, while guaranteeing the sufficient

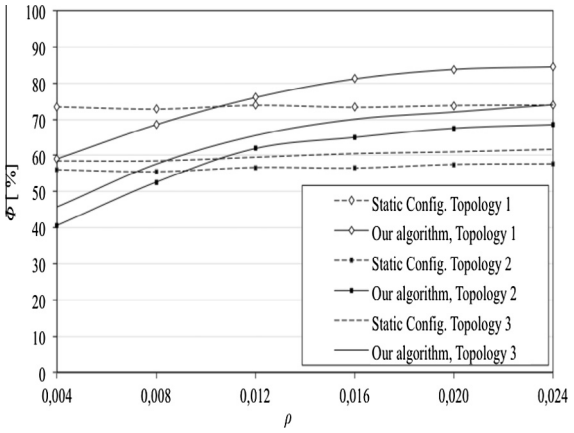

Fig. 6. Percentage of users served by FBSs (Φ) vs. UE's density ρ.

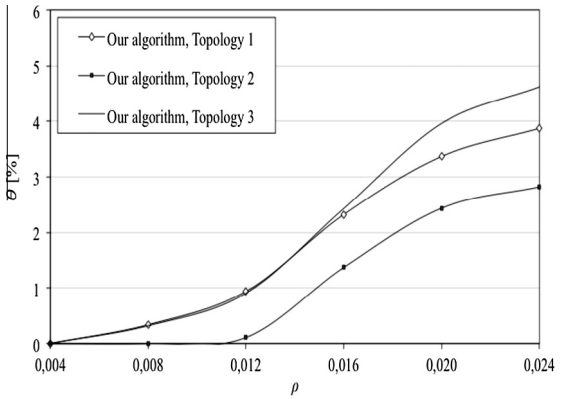

Fig. 7. Overlapping factor of femtocell (Θ) vs. UE's density ρ.

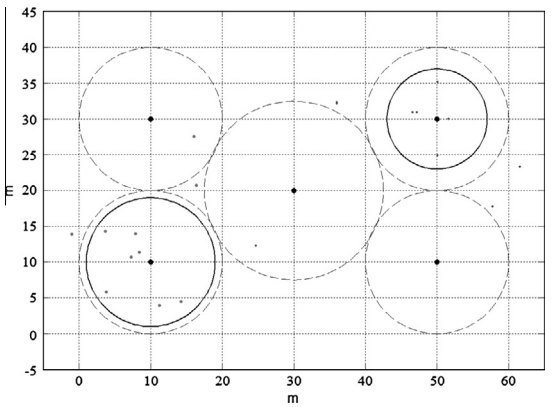

Fig. 8. Static coverage (dotted line) and final configuration for the proposed algorithm (solid line), $N_u = 20$.

SINR level to all connected users (minimal overlap). So, in a high load scenario our algorithm allows to offload more traffic from the MBS and therefore to increase the overall system capacity. In addition, EE of the overall cellular network also enhances, as MBS's power consumption is strongly related to its traffic load [23]. Let's note that

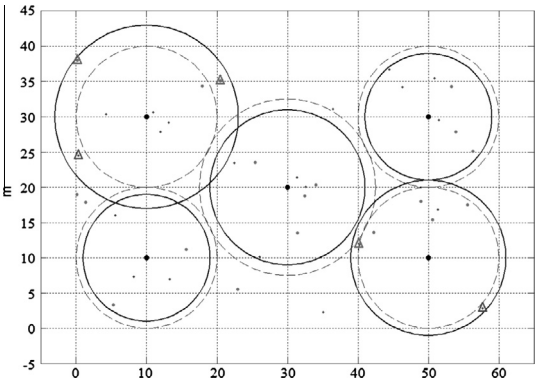

Fig. 9. Static coverage (dotted line) and final configuration for the proposed algorithm (solid line), $N_u = 40$.

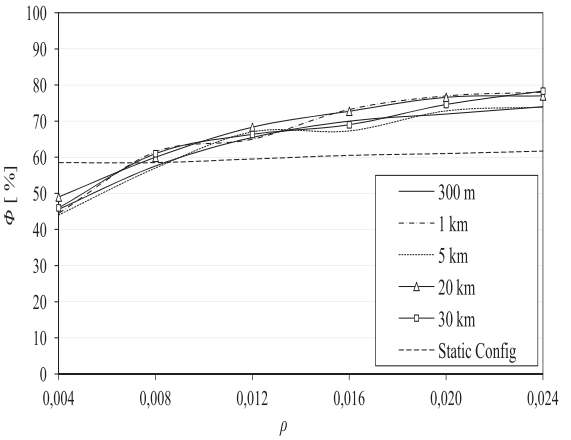

Fig. 10. Φ vs. ρ at various distance of the group of FBSs from the MBS – Topology 3.

numerical values vary depending on the specific arrangement of FBSs, but, regardless the network topology being considered, implementation of the proposed algorithm allows to offload up to 13% active users from the MBS. This confirms scalability of proposed power control scheme.

Lastly, for each topology, we have considered various distances of the FBSs from the MBS (300 m, 1 km, 5 km, 20 km and 30 km). The simulation results differ slightly from those previous (e.g. as shown in Fig. 10 for Topology 3) confirming flexibility and robustness of our self-coverage function.

Finally, the scalability, dynamic adaptability, and flexibility of the proposed algorithm guarantee a natural robustness to any faults or shutdown of one or more FBSs.

4.4. Multi-MBS environment

To evaluate the behavior of our control scheme in a multi-MBS environment, we assess the impact of the presence of neighboring MBS on estimation of the decision-making parameters (*NOISE_UL* and *PSINR*).

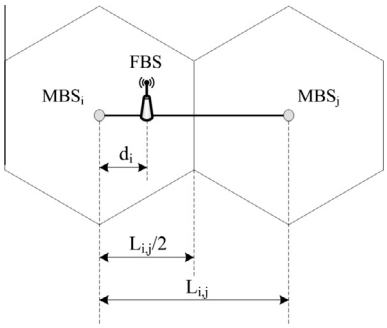

Fig. 11. Multi-MBS simulation scenario.

We have considered two adjacent MBSs: MBS$_i$ and MBS$_j$, which belong to the same operator and have equal maximal transmit powers P_t^{MBS} (see Table 2). The MBSs are located at the distance $L_{i,j}$ from each other. In the coverage area of MBS$_i$ is embedded a FBS at the distance d_i from it (see Fig. 11).

NOISE_UL represents the total noise power in the uplink frequency band measured by the FBS, therefore the transmission power of the interfering neighboring MBS can non affect directly. What may happen is that the idle FBS, located at the edge of macrocell MBS$_i$, would switch to Active State due to the noise generated by transmissions of UEs connected to different MBSs (MBS$_i$ and MBS$_j$). However, it will not cause any negative effect on the operation of our algorithm as it does not foresee any signaling exchange with MBSs. On the contrary, at the edges of the cell, where users experience the worst conditions in terms of channel quality and bandwidth, femtocells will be switched on providing better performance to all users.

As regards the impact of adjacent MBS on the second decision-making parameter (*PSINR*), we have assessed the downlink interference experienced by a femtocell user due to the pilot transmissions of both MBSs (I_{MBS_i} and I_{MBS_j}), singly and in the aggregate, for several distance values d_i.[1] In particular, we have considered a worst-case, where the distance d_i increases from one MBS by Δd, while the distance from the other MBS decreased by equal value (Δd) and the interfering effect becomes more severe.

In Fig. 12, for $L_{ij} = 3$ km, the simulation results show that for low d_i values, that is the FBS is close to MBS$_i$, the interference power that receives a femtocell UE from neighboring MBS$_j$ (I_{MBS_j}) is negligible compared to those from MBS$_i$ (I_{MBS_i}). Obviously, the interference power, I_{MBS_j}, reaches its maximal value if the femtocell is located at the cell edge, $d_i = L_{ij}/2$. Here, the aggregate MBSs' interference ($I_{MBS_i} + I_{MBS_j}$) doubles, but it is lower than the interference level that a user experiences when it is connected to a FBS located next to one of MBSs ($d_i = 100$ m in Fig. 12). Besides $L_{ij} = 3$ km we have considered also other L_{ij} values ($L_{ij} = \{2, 5, 10\}$ km) obtaining analogous results.

[1] As the femtocell radius is very small, we approximate the distance between femto UE and the MBS$_i$ with d_i.

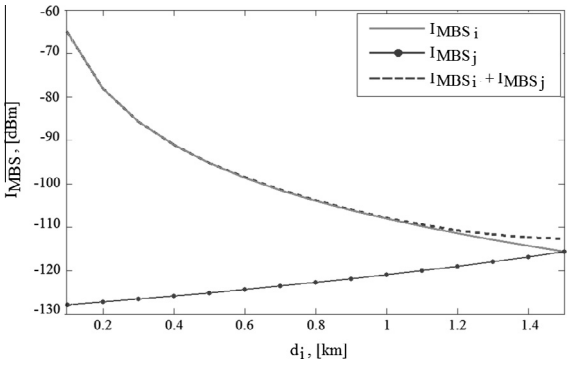

Fig. 12. Interference power received from MBS$_i$ and MBS$_j$ vs. distance from MBS$_i$.

In conclusion, the simulation results and the above analysis show that the presence of neighboring MBS does not cause negative effects in the estimation of both decision-making parameters. We infer that the behavior of our pilot power control scheme is not deteriorated due to the presence of neighboring MBS, so we expect that it operates properly also in a multi-MBS environment.

4.5. Evaluation of stability

The performance of our algorithm, in terms of stability and responsiveness of the control, depends on the ΔT value, that is the time interval in which a FBS resides in Stabilization State before switching to Dynamic Power Adaption procedure.

We expect that with shorter ΔT duration the system is more responsive to the changes of traffic conditions due to the frequent pilot power adaptions. But this could result in a significant increase in the number of handover events. To determine the appropriate ΔT value, we have considered a new scenario in which the traffic load is variable in time. More specifically, the simulations have been carried out under the following assumptions:

(1) UEs are uniformly distributed in the considered macrocell area. The total number of UEs varies during the observation period of 16 h (6:00–22:00) as shown in Fig. 13.
(2) The mobility of UEs is neglected, but each UE can reside in on/off state following the Poisson Distribution process of the call arrival time. The interarrival time and the call holding time are exponentially distributed with means $\lambda = 4$ min and $\mu = 3$ min respectively.

Due to the limit of space, we provide simulation results only for Topology 1, but analogous results were obtained also with others.

Fig. 14 shows the average percentage of users covered by all FBSs during the whole observation period for several ΔT values. We observe that for $\Delta T \leqslant 16.5$ min our algorithm responds more efficiently to the traffic fluctuations and, consequently, provide higher Φ values compared to

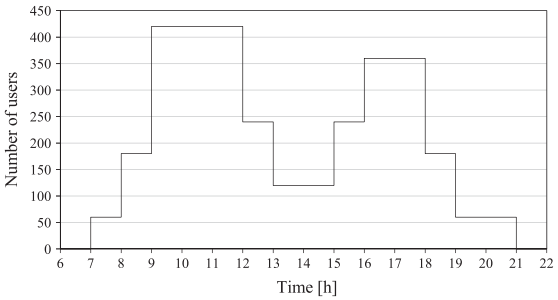

Fig. 13. User distribution pattern.

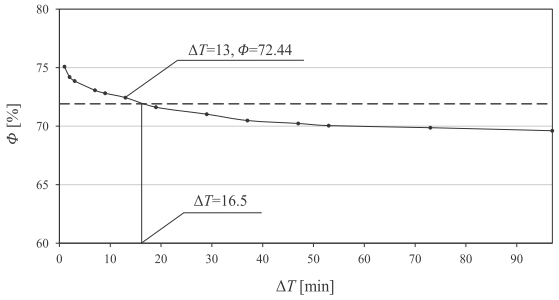

Fig. 14. Φ vs. ΔT intervals.

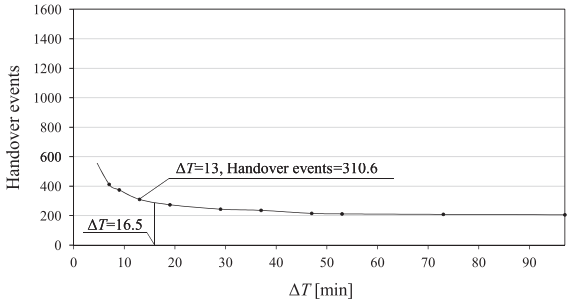

Fig. 15. The total number of handover events vs. ΔT intervals.

the static configuration (dotted line). However, such ΔT values lead to a substantially increased number of handovers (see Fig. 15) due to the frequent pilot power calibration events in attempt to continuously improve the coverage. Protracted ΔT duration delays the response of FBSs to the changes of the traffic demand and, as a consequence, adversely affect the performance of our algorithm in terms of Φ (see Fig. 14 for $\Delta T > 16.5$ min). Nevertheless, in this case the number of handovers is significantly reduced (see Fig. 15).

Let's also note that the total duration of Listen Mode intervals is not sensitive to ΔT values, as the FBS switches to Listen Mode if no UE is connected to it independently if ΔT is expired or not.

So, by comparative analysis of simulation results shown in Figs. 14 and 15 we have determined $\Delta T = 13$ min as an optimal value, that permits to achieve a trade-off between the number of handover events and Φ. The subsequent analysis is made with $\Delta T = 13$ min.

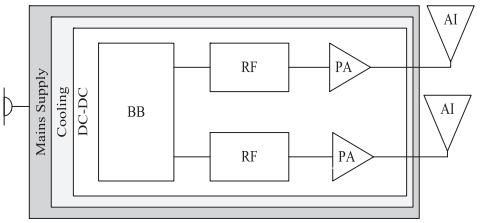

Fig. 16. Overview of base station components included in the power model.

4.6. Evaluation of energy efficiency

In the following we provide a power consumption analysis for FBS which operates in Active Mode and Listen Mode. According to [23] the power consumption is load dependent for MBSs, while there is a negligible load dependency for FBSs, so we assume static power consumption across all traffic load for FBSs and we use a static component-based power consumption evaluation model introduced in [26]. This power model is built around the split of a BS into a number of components and sub-components, as shown in Fig. 16.

A FBS consists of two transceivers (TRXs). A TRX comprises an Antenna Interface (AI), a Power Amplifier (PA), a Radio Frequency (RF) small-signal transceiver section, a digital baseband (BB) interface including a receiver and transmitter section, a DC–DC power supply, an active cooling system and an AC–DC unit (Main Supply) for connection to electrical power grid.

So, the power consumption of the FBS that resides in Active Mode can be calculated as follows

$$P_{ACT} = N_{TRX} \cdot \frac{P_{PA} + P_{RX} + P_{TX} + P_{BB} + P_{Sniff.}}{(1 - \sigma_{DC})(1 - \sigma_{MS})(1 - \sigma_{Cool.})}. \quad (6)$$

Table 3 summarizes the state of the art power consumption of LTE femtocells as of 2012. Applying the data reported in Table 3 to Eq. (6), we obtain $P_{ACT} = 7$ W.

Table 3
LTE femtocell transceiver power consumption.

PA (W)	TX (W)	RX (W)	BB (W)	DC–DC, σ_{DC}	Cooling, σ_{Cool}	AC–DC, σ_{MS}	N_{TRX}
1.0	0.2	0.2	1.2	0.08	0.0	0.1	2

By switching to Listen Mode, the FBS switches off the PA, RF transmitter and RF receiver. However, the sniffer ($P_{Sniff.} = 0.3$ W [4]) is switched on to perform received power measurements on the uplink frequency band. So, the power consumption of the FBS that resides in Listen Mode results

$$P_{LM} = N_{TRX} \cdot \frac{P_{BB} + P_{Sniff.}}{(1-\sigma_{DC})(1-\sigma_{MS})(1-\sigma_{Cool.})} = 3.62 \text{ W}. \quad (7)$$

As can be estimated, the addition of Listen Mode to the normal femtocell operation results in a power saving of 48.29% for each idle femtocell.

The total amount of energy consumed by FBS_k is given in the following equation:

$$E^k_{FBS} = P_{ACT,k} \cdot t_{ACT,k} + P_{LM,k} \cdot t_{LM,k}, \quad (8)$$

where $P_{ACT,k}$ and $P_{LM,k}$ represent the power consumption of FBS_k when it resides in Active or in Listen Mode, respectively; $t_{ACT,k}$ and $t_{LM,k}$ represent the time period (expressed in hours) in which the FBS_k is in Active Mode and in Listen Mode, respectively.

So, the total amount of energy consumed by entire femtocell network can be calculated as:

$$E_{FN} = \sum_{k=1}^{N} E^k_{FBS}. \quad (9)$$

To evaluate the energy saving potential of our algorithm in a realistic scenario we have taken into account a traffic profile that emulates the spatial and temporal variations during a working day in an enterprise scenario. More specifically, we consider Topology 3 (Fig. 17) provisioned of a Dining and Lounge Area, where the number of users increases substantially during the lunch break (from 13:00 to 15:00) (as shown in Fig. 18).

After a series of simulations, in Fig. 19 we report the number of active femtocells, averaged over each hour. Besides, in Fig. 20 the average number of active users connected to FBSs with our algorithm and those with the static configuration are presented. Finally, in Fig. 21 we report the energy saving gain obtained for each hour and calculated as follows

$$E_{GAIN} = \frac{E_{FN,Static} - E_{FN,\ Our\ Approach}}{E_{FN,\ Static}}, \quad (10)$$

where $E_{FN,Static}$ and $E_{FN,OurApproach}$ are calculated according to (9) and represent the total amount of energy consumed by the whole femtocell network with the static configuration and with implementation of our algorithm, respectively.

By comparing the above results, in low load conditions numerous FBSs reside in Listen Mode, that permits to achieve a significant energy gain (see Fig. 21) and in the same time does not affect seriously the user coverage. In fact, as shown in Fig. 20, the coverage provided by our power control scheme is only marginally lower than those static. Nevertheless, in these conditions the MBS alone can provide satisfactory performance to its connected users. In high load conditions, most of FBSs are active and our control scheme provides better coverage compared to the

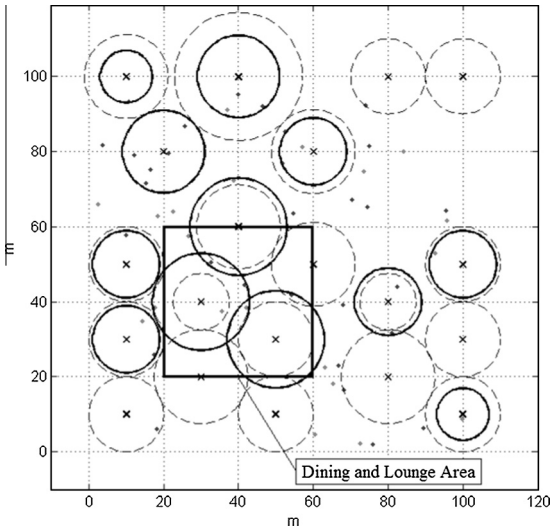

Fig. 17. Static configuration (dotted line) and final coverage for our algorithm (solid line) – Topology 3, $\rho = 0.006$.

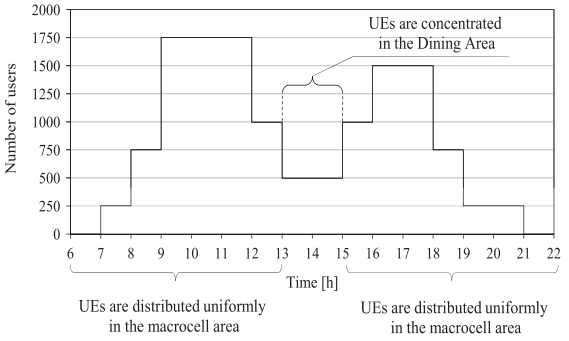

Fig. 18. User distribution pattern.

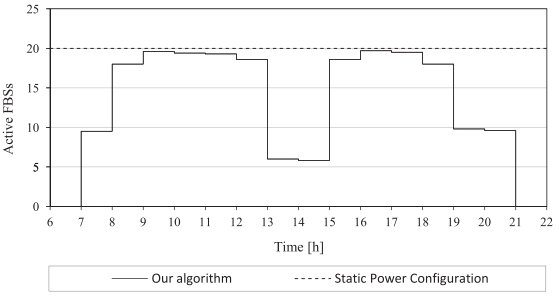

Fig. 19. Medium number of active femtocells vs. time.

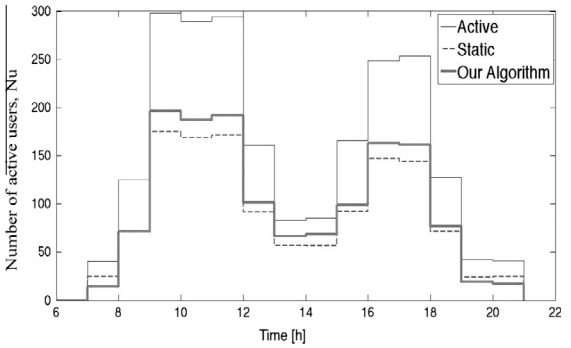

Fig. 20. Percentage of users served by FBSs (ϕ) vs. Time of day.

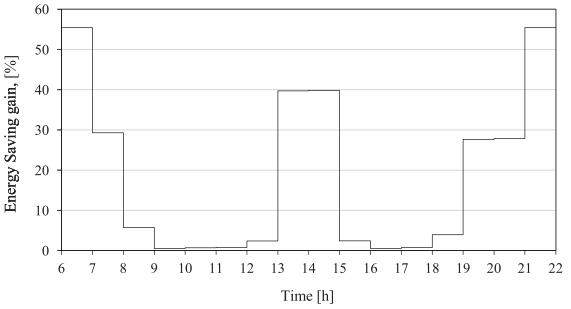

Fig. 21. Energy saving gain vs. time of day.

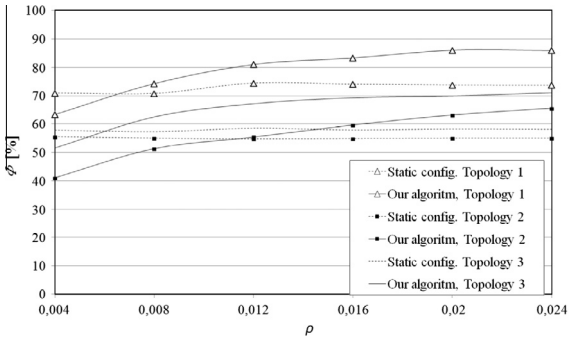

Fig. 22. Percentage of users served by FBSs (Φ) vs. UE's density ρ using the path loss models (11) and (12).

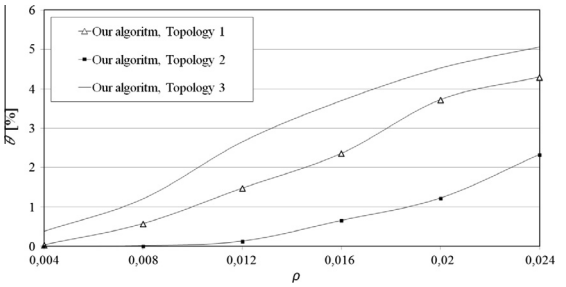

Fig. 23. Overlapping factor of femtocell (Θ) vs. UE's density ρ using the path loss models (11) and (12).

static configuration (Fig. 20) and, consequently, more traffic is offloaded from the MBS (just when it is the most necessary).

Applying (10) to the whole observation period, we have quantified the total amount of energy consumed by entire femtocell network during a working day: $E_{FN,Static} = 2240.00$ Wh and $E_{FN,OurApproach} = 1871.84$ Wh. It can be estimated that implementation of our algorithm in this case study results in an overall energy saving gain of 16.44%. It is important to emphasize that the total power saving of the femtocell network is relevant considering the expected large-scale deployment of FBSs in urban scenarios.

4.7. Different path loss models

Path loss models are good instruments and are widely used for estimation of the overall network capacity, for testing various control schemes, etc., but they depend on multiple environmental factors and several models are proposed in the literature. So far we have used a unique path loss model between UE and MBS or FBS [27].

In the following we verify if our algorithm operates properly in other radio propagation environments using different path loss models. For example, for a suburban scenario, the path loss between an indoor UE_u and the outdoor MBS can be modeled as follows [28]:

$$PL_{NLOS}(d_{u,MBS}) = 2.7 + 42.8 \cdot \log 10(d_{u,MBS}) + L_{OW}, \qquad (11)$$

where *NLOS* denotes that there is no visual line of sight between transmitter and receiver; $d_{u,MBS}$ is a distance between UE_u and the MBS; L_{OW} is the penetration loss of an outdoor wall and we assume $L_{OW} = 20$ dB.

The path loss between indoor UE_u and the FBS_j that are in the same building, can be calculated as

$$PL(d_{u,j}) = 38.46 + 20 \cdot \log 10(d_{u,j}) + 0.7 \cdot d_{2D,indoor} + 18.3 \cdot n^{((n+2)/(n+1)-0.46)}, \qquad (12)$$

where $(d_{u,j})$ is a distance between UE_u and the FBS_j; $(0.7 \cdot d_{2D,indoor})$ takes account of penetration loss due to the walls inside an apartment, $d_{2D,indoor}$ is a thickness of an indoor wall and it is assumed $d_{2D,indoor} = 0.3$ m; n is the number of penetrated floors and we consider $n = 1$.

With these path loss models we have derived the suited *NOISE_TH* value and evaluated the behavior of our algorithm for all the cases considered previously. We can compare the results in Fig. 22 with those in Fig. 6 and in Fig. 23 with those in Fig. 7. For example, for the case study of paragraph 4.6, the control algorithm obtains an energy saving of about 16% as before. Other results are not reported only due limited space but the simulation results does not differ from those already obtained, showing so that our algorithm runs well any path loss model is used to simulate the propagation environment.

5. Conclusion

Enterprise femtocell deployment will be large-scale and it will cover a wide range of environments in public areas such as enterprise buildings, airports and shopping malls. For this scenario, where the open access mode is used, we propose a self-organizing measurement-based coverage function for LTE FBSs embedded in a macrocell area that addresses both power consumption reduction and femto–femto interference issues. Our solution provides scalable, robust and stable control without any signaling overhead compared to centralized approaches.

In a low load scenario our pilot power control scheme places some FBSs in Listen Mode, that permits to reduce power consumption to up to 48.29% for each idle femtocell. In a high load scenario each FBS dynamically adapts its pilot power (and thus the coverage) to the on-site traffic demand and in these conditions our algorithm permits to offload up to 13% more active users from the MBS to FBSs compared to the static configuration scheme while providing an acceptable QoS to all connected users. Furthermore, we use a component-based model to quantify the energy saving potential of our algorithm. Simulation results show that in a case study our approach achieves an overall energy saving gain of 16.44% under a typical enterprise traffic profile.

We also address the implementation issues of our control scheme discussing in detail the estimation of two decision-making parameters. We show that some measurements are defined by LTE specifications and that the sniffing capability is already integrated without additional costs in some FBSs produced by key vendors.

The target of our further research is to extend the functionality of the proposed algorithm considering a "Hybrid access mode" for FBSs, in which the femtocell provides service to all UEs, but preferential treatment is given to its associated registered users, while other users can connect via a subset of remaining available subchannels on a best-effort basis. Furthermore, we will analyze the cost of increased number of handovers due to the femtocell pilot power calibration.

Acknowledgments

The authors would like to thank the anonymous reviewers for their comments and constructive criticism which greatly helped to clarify and improve the presentation of this paper.

Appendix A. Noise level on the uplink frequency band

The noise level on the uplink frequency band measured by FBS is calculated as

$$NOISE\_UL_k = \sum_{u=1}^{N_u} (P_u - PL(d_{u,k})), \tag{A.1}$$

where N_u is a total number of active users in the macrocell area, P_u represents the transmit power of UE_u, $PL(d_{u,k})$ is a path loss between UE_u and FBS_k.

The 3GPP specifications [25] define the setting of the UE_u transmit power by the following equation (dB scale):

$$P_u = min(P_{max}, 10 \cdot \lg(M_u) + P_0 + \alpha \cdot PL(d_{u,j}) + \Delta_{MCS} + f(\Delta_i)), \tag{A.2}$$

where P_{max} is the maximum allowed transmit power that depends on the UE power class; M_u is the number of assigned Physical Resource Blocks (PRBs) to UE_u; P_0 is a UE specific (optionally cell specific) parameter that represents the power allocated to one PRB; α is a cell specific path loss compensation factor; $PL(d_{u,j})$ is the downlink path loss between UE_u and its serving FBS_j, calculated in the UE_u; Δ_{MCS} is a UE specific parameter depending on the Modulation and Coding Scheme (MCS); $f(\Delta_i)$ is a function that allows relative, cumulative and absolute corrections and it is also UE specific.

Neglecting the short term variations (Δ_{MCS} and $f(\Delta_i)$) in (A.2), the average transmit power level of UE_u becomes:

$$P_u = min(P_{max}, 10 \cdot \lg(M_u) + P_0 + \alpha \cdot PL(d_{u,j})). \tag{A.3}$$

The path loss (in dB) is modeled as [27]

$$PL(d_{u,j}) = A_s + 10 \cdot n \cdot \lg(d_{u,j}) + L_w, \tag{A.4}$$

where A_s is a path loss at 1 m; n is a path loss exponent; $(d_{u,j})$ is a distance between UE_u and FBS_j; L_w is a wall penetration loss.

As regards the practical implementation of *NOISE_UL* estimation, each FBS must be equipped with a sniffer, that is an additional receiver that can perform correlation between signals in uplink. This receiver is as those already provided in the FBS to receive uplink traffic (operates in the same frequency band), so the duplication of an uplink receiver would bring a negligible extra cost. In fact, the sniffing capability is often already integrated into FBSs. The key vendors produce LTE FBSs equipped with a Network Listen Module (NLM) which facilitates the plug-and-play deployment of femtocells (see Table A.4). It permits to the FBS to make measurements of surrounding macrocells and femtocells in order to optimize its configuration settings. NLM can be used in our approach to perform measurements of *NOISE_UL* and since the module is already integrated into the femtocell such a solution incurs no extra cost.

Table A.4
Femtocell BS equipped with NLM.

Vendor	Product name
ip.access Limited	nanoLTE Access Points family (femtocells for enterprise and public access): nanoLTE E–40, nanoLTE+ E–100
Cisco Systems	Cisco Aironet 3600 Series and Cisco Universal Small Cell 5310
Alcatel-Lucent	9760 Small Cell product family
Fujitsu	BroadOne LS100 Series LTE femtocell (residential), BroadOne LS200 Series LTE femtocell (semi-public/enterprise)

Appendix B. Pilot signal to interference plus Noise Ratio

Our approach is to reduce the effects of femto–femto interference calibrating the coverage of FBSs in order to minimize the overlap between adjacent femtocells. As the coverage area of a BSs is defined by the strength of its pilot signals, we have introduced the *PSINR* parameter (Pilot Signal to Interference plus Noise Ratio). It is calculated for each active UE_u connected to the FBS_k ($PSINR_u^k$) as the ratio between the power of pilot signal received from its serving cell and interfering pilot signals received from the neighboring cells:

$$PSINR_u^k = \frac{P_{r,u}^k}{I_u^k + N_0}, \tag{B.1}$$

where $P_{r,u}^k$ is the pilot power of FBS_k measured by UE_u; I_u^k is the interference of other cells; N_0 is a thermal noise power.

Below we provide analytic expressions for calculation of the terms in (B.1).

The FBS_k pilot power measured by UE_u is modeled as

$$P_{r,u}^k = \frac{P_{t,u}^k}{A_s \cdot L_w \cdot d_{u,k}^n}, \tag{B.2}$$

where $P_{t,u}^k$ is pilot power transmitted by FBS_k and $d_{u,k}^n$ is a distance between UE_u and FBS_k.

The interference power measured by UE_u due to the pilot signals transmission of all non-serving BSs (macro and femto) can be calculated as

$$I_u^k = \sum_{j=1, j\neq k}^{N+1} P_{r,u}^j, \tag{B.3}$$

where N is the total number of FBSs; $P_{r,u}^j$ is the pilot power received from interfering BS_j (calculated according to (B.2)).

Note that because of "Assumption 1" of no intra-cell downlink interference, the pilot power transmitted by the serving FBS is not seen as interference by UE_u.

The FBS_k has to ensure that no UE's *PSINR* falls below its threshold *PSINR_TH* level chosen to provide an acceptable QoS level. So, the second decision-making parameter represents the minimal value of the set $\{PSINR_u^k\}$:

$$PSINR_k = min\{PSINR_u^k\}, \quad \forall u \in U_k, \tag{B.4}$$

where U_k is the number of active users connected to the FBS_k.

As regards the practical implementation of *PSINR* estimation, let's note that LTE specifications define the Reference Signal Received Power (RSRP) measurement made by UEs. It is a type of signal strength measurement and is indicative of the cell coverage. RSRP is defined as the linear average over the power contributions (in (W)) of all resource elements that carry cell-specific Reference Signals (RSs) (or pilot signals) within the operating bandwidth. It is used in LTE for cell reselection and handover and therefore is considered to be the most important measurement quantity. Each active UE estimates RSRP in the serving cell and neighboring cells. The measurement results are reported to the serving cell in order to aid in handover procedure. The measurement reporting mechanism can be configured by the serving cell and it can be periodic (the connected UE can be instructed to send RSRP measurements periodically) or event-triggered (the connected UE sends RSRP measurements when it is requested by its serving cell). With this information FBSs can anytime estimate the *PSINR* value needed for the proposed control mechanism [13].

Let's note that due to the importance of cell specific RSs, they are the highest powered components within the downlink signal. So, based on how we have defined the formula for *PSINR* calculation (B.1), this value is equivalent to the worst SINR value that the user would experience if he is using an resource element that is simultaneously allocated and used in the neighboring cells.

References

[1] D. Mavrakis, Small Cell Market Status, Tech. Rep. 050, Informa Telecoms&Media, London, UK, 2013.

[2] H. Claussen, I. Ashraf, L.T.W. Ho, Dynamic idle mode procedures for femtocells, Bell Labs Tech. J. 15 (2) (2010) 95–116.

[3] I. Ashraf, F. Boccardi, L. Ho, SLEEP mode techniques for small cell deployments, IEEE Commun. Mag. 49 (8) (2011) 72–79.

[4] I. Ashraf, L.T.W. Ho, H. Claussen, Improving energy efficiency of femtocell base stations via user activity detection, in: IEEE Wireless Communications and Networking Conference (WCNC), 2010, pp. 1–5.

[5] H.-S. Jo, C. Mun, J. Moon, J.-G. Yook, Self-optimized coverage coordination in femtocell networks, IEEE Trans. Wireless Commun. 9 (10) (2010) 2977–2982.

[6] I. Ashraf, H. Claussen, L.T.W. Ho, Distributed radio coverage optimization in enterprise femtocell networks, in: IEEE International Conference on Communications (ICC), 2010, pp. 1–6.

[7] S. Al-Rubaye, A. Al-Dulaimi, J. Cosmas, Pilot power optimization for autonomous femtocell networks, in: Wireless Advanced (WiAd), 2011, pp. 170–175.

[8] M. Lin, T. La Porta, Dynamic interference management in femtocells, in: 21st International Conference on Computer Communications and Networks (ICCCN), 2012, pp. 1–9.

[9] A. Dudnikova, D. Panno, An energy saving approach for femtocell coverage function, in: 22nd ITC Specialist Seminar on Energy Efficient and Green Networking (SSEEGN), 2013, pp. 7–12.

[10] A. Dudnikova, D. Panno, A fully distributed algorithm for pilot power control in LTE femtocell networks, in: Wireless Days (WD), 2013, pp. 1–3.

[11] Y. Li, Z. Feng, S. Chen, Y. Chen, D. Xu, P. Zhang, Q. Zhang, Radio resource management for public femtocell networks, EURASIP J. Wireless Commun. Networking 2011 (1) (2011) 1–16.

[12] S.R. Saunders et al., Femtocell networks and architectures, Femtocell Communications and Technologies: Business Opportunities and Deployment Challenges, vol. 109, Wiley, West Sussex, UK, 2009.

[13] S. Sesia, I. Toufik, M. Baker, LTE-The UMTS Long Term Evolution: From Theory to Practice, 2nd ed., west sussex ed., Wiley, UK, 2011. pp. 478–482, (Chapter Small Signal Requirements).

[14] M. Şahin, I. Guvenc, M.-R. Jeong, H. Arslan, Handling CCI and ICI in OFDMA femtocell networks through frequency scheduling, IEEE Trans. Consumer Electron. 55 (4) (2009) 1936–1944.

[15] T.-H. Kim, T.-J. Lee, Throughput enhancement of macro and femto networks by frequency reuse and pilot sensing, in: Proc. IEEE International Performance, Computing and Communications Conference (IPCCC), 2008, pp. 390–394.

[16] P. Lee, T. Lee, J. Jeong, J. Shin, Interference management in LTE femtocell systems using fractional frequency reuse, in: The 12th International Conference on Advanced Communication Technology (ICACT), vol. 2, 2010, pp. 1047–1051.

[17] A. Ahmedin, A. Elsherif, X. Liu, J. Hamalainen, R. Wichman, Macrocell resource adaptation for improved femtocell deployment and interference management, in: 2014 World Congress on Computer Applications and Information Systems (WCCAIS), 2014, pp. 1–6.

[18] S. Saleem, H. King, Avoidance of co-tier interference between femtocells with different access modes, Int. J. Inf. 2 (8) (2012).

[19] S. Lin, H. Tian, Clustering based interference management for QoS guarantees in OFDMA femtocell, in: Wireless Communications and Networking Conference (WCNC), 2013 IEEE, IEEE, 2013, pp. 649–654.
[20] P. Mach, Z. Becvar, Centralized dynamic resource allocation scheme for femtocells exploiting graph theory approach, in: Wireless Communications and Networking Conference (WCNC), 2014 IEEE, IEEE, 2014, pp. 1479–1484.
[21] T. Ma, P. Pietzuch, Femtocell coverage optimisation using statistical verification, in: NETWORKING 2011, Springer, 2011, pp. 343–354.
[22] L. Mohjazi, M. Al-Qutayri, H. Barada, K. Poon, Femtocell coverage optimization using genetic algorithm, in: Telecom World (ITU WT), 2011 Technical Symposium at ITU, IEEE, 2011, pp. 159–164.
[23] M. Obaidat, A. Anpalagan, I. Woungang, Handbook of Green Information and Communication Systems, 1st ed., waltham ed., Academic Press, 2012. pp. 20–26 (Chapter Cognitive strategies for green two-tier cellular networks).
[24] H. Claussen, L.T.W. Ho, L. Samuel, Self-Optimization of coverage for femtocell deployments, in: Wireless Telecommunications Symposium (WTS), 2008, pp. 278–285.
[25] 3GPP, Technical Specification Group Radio Access Network; Evolved Universal Terrestrial Radio Access (E-UTRA); Physical layer procedures (Release 10), TS 36.213 v.10.0.0 Release 10, 3GPP, 2010.
[26] G. Auer, O. Blume, V. Giannini, I. Godor, M. Imran, Y. Jading, E. Katranaras, M. Olsson, D. Sabella, P. Skillermark, et al., Energy Efficiency Analysis of the Reference Systems, Areas of Improvements and Target Breakdown, EARTH.
[27] F. Mhiri, K. Sethom, R. Bouallegue, G. Pujolle, AdaC: adaptive coverage coordination scheme in femtocell networks, in: Wireless and Mobile Networking Conference (WMNC), 2011 4th Joint IFIP, 2011, pp. 1–7.
[28] 3GPP, Technical Specification Group Radio Access Network; Evolved Universal Terrestrial Radio Access (E-UTRA); Further advancements for E-UTRA physical layer aspects (Rel. 9), TR 36.814 v. 9.0.0, 3GPP, 2010.

Anna Dudnikova was born in 1989 in Tomsk, Russia. In June 2011 graduated with honors from the Tomsk State University of Control Systems and Radio electronics with the qualification of an engineer in "Radio communication, broadcasting and television". After graduation she moved to Italy and from October 2011 she is a Ph.D. student of the department of Electric, Electronic and Computer Engineering at the University of Catania. Her primary research area is management of LTE and LTE-Advanced femtocell networks.

Daniela Panno received the Laurea degree in electrical engineering and the Ph.D. degree in electronic and computer science from the University of Catania, Catania, Italy, in 1989 and 1993, respectively. Currently, she is an Associate Professor of Telecommunications at the Engineering Faculty, University of Catania. She has served as Guest Editor for *Computer Communications Special Issues on Computational Intelligence in Telecommunications Networks* (October 2002). Her recent research interests include traffic management and performance evaluation in high-speed and in wireless networks, soft computing application in the field of telecommunications.

Antonio Mastrosimone received his master's degree in Telecommunication Engineering with honors in October 2013 from the University of Catania where he is a Ph.D. Student of the Department of Electric, Electronic and Computer Science Engineering. His research focuses on issues related to wireless sensor network and energy saving in mobile cellular network of IV generation.